

# Models of gravitational lens candidates from Space Warps CFHTLS

Rafael Küng,<sup>1</sup> Prasenjit Saha,<sup>1</sup> Ignacio Ferreras,<sup>2</sup> Elisabeth Baeten,<sup>3</sup> Jonathan Coles,<sup>4</sup> Claude Cornen,<sup>3</sup> Christine Macmillan,<sup>3</sup> Phil Marshall,<sup>5</sup> Anupreeta More,<sup>6</sup> Lucy Oswald<sup>7</sup> Aprajita Verma<sup>8</sup> and Julianne K. Wilcox<sup>3</sup>

<sup>1</sup>Physik-Institut, University of Zurich, Winterthurerstrasse 190, 8057 Zurich, Switzerland

<sup>2</sup>Mullard Space Science Laboratory, University College London, Holmbury St Mary, Dorking, Surrey RH5 6NT, UK

<sup>3</sup>Zooniverse, c/o Astrophysics Department, University of Oxford, Oxford OX1 3RH, UK

<sup>4</sup>Physik-Department, Technische Universität München James-Franck-Str. 1, 85748 Garching, Germany

<sup>5</sup>Kavli Institute for Particle Astrophysics and Cosmology, Stanford University, 452 Lomita Mall, Stanford, CA 94035, USA

<sup>6</sup>Kavli IPMU (WPI), UTIAS, University of Tokyo, Kashiwa, Chiba 277-8583, Japan

<sup>7</sup>Murray Edwards College, University of Cambridge, Cambridge CB3 0DF, UK

<sup>8</sup>Sub-department of Astrophysics, University of Oxford, Denys Wilkinson Building, Keble Road, Oxford, OX1 3RH, UK

Accepted XXX. Received YYY; in original form ZZZ

## ABSTRACT

We report modelling follow-up of recently-discovered gravitational-lens candidates in the Canada France Hawaii Telescope Legacy Survey. Lens modelling was done by a small group of specially-interested volunteers from the Space Warps citizen-science community who originally found the candidate lenses. Models are categorised according to seven diagnostics indicating (a) the image morphology and how clear or indistinct it is, (b) whether the mass map and synthetic lensed image appear to be plausible, and (c) how the lens-model mass compares with ~~compares with the the stellar mass and the abundance-matched halo mass derived from photometry of the lensing galaxy.~~

~~The lens-model. The lensing masses range from  $\sim 10^{11} M_{\odot}$  to  $> 10^{13} M_{\odot}$ . Preliminary estimates of the stellar masses show (with two outliers) a smaller spread in stellar mass (except for two lenses); a factor of a few below or above  $\sim 10^{11} M_{\odot}$ . That is, the stellar-mass fraction declines. Therefore, we expect the stellar-to-total mass fraction to decline sharply as lensing mass increases. The highest-mass-most massive system with a convincing model is J1434+522 (SW 05). The two low-mass outliers are J0206-095 (SW 19) and J2217+015 (SW 42); if these two are indeed lenses, they are probing probe an interesting regime of very low star-formation efficiency. Some improvements to the modelling software used (SpaghettiLens), and discussion of strategies for regarding scaling to future surveys with more and frequent discoveries, are also included.~~

**Key words:** gravitational lensing: strong – galaxies: general – ~~galaxies: stellar content – dark matter~~

## 1 INTRODUCTION

By a curious coincidence, the typical escape velocity of massive galaxies ~~of order a few hundred km/s~~ is such that  $v_{\text{esc}}^2/c^2$ , expressed as an angular distance, is comparable to the apparent sizes of ~~a~~-galaxies at cosmological distances. This coincidence is fortunate, because it makes the ~~gravitational~~ lensing deflection angle (~~which is  $2v_{\text{esc}}^2/c^2$~~ ) of distant galaxies ( $\alpha \sim 2v_{\text{esc}}^2/c^2$ ) comparable to their size on the sky, ~~and as~~. As a result, strong lensing by galaxies ~~tends to produce~~ produces images that probe ~~the dark halos of~~

~~those galaxies. This is important, because while their host dark matter halos, providing a useful tool to understand galaxy formation. While there is a general consensus that basic mechanism of galaxy formation involves about the basic mechanisms at play, involving gravitational collapse, fragmentation, and mergers of dark-matter clumps, into which gas fell, cooling through radiative processes to form dense clouds and eventually stars, there is much debate about the details (for a summary, see Silk & Mamon 2012). In particular, the nature of dark matter remains mysterious: most researchers take it to be a collisionless non-relativistic fluid~~

(cold dark matter or CDM) readily studied by simulations (for example, the influential millenium simulation by Springel et al. 2005). But other (for example, the influential Millennium simulation, However, alternative scenarios, where dark matter has exotic dynamical properties (Saxton & Ferreras 2010; Schive et al. 2016), or is not really matter at all, but a modification of gravity (McGaugh et al. 2016), have also been considered.

All this motivates using galaxy lenses—the use of strong gravitational lensing over galaxy scales to study the mutual dynamics of dark matter, gas and stars in galaxies. Several studies in recent years have done so (Koopmans et al. 2009; Leier et al. 2011, 2012, 2016; Bruderer et al. 2012) it is desirable to enlarge the samples from tens of lensing galaxies to thousands. Doing so requires both finding more lenses and also modelling their mass distribution. Recent searches through the CFHTLS (Cuillandre et al. 2012) CFHT Lens Survey (CFHTLS Heymans et al. 2012) using arc-finders (e.g., More et al. 2012; Maturi et al. 2014; Gavazzi et al. 2014; Sonnenfeld et al. 2017) by machine learning (e.g., Paraficz et al. 2016; Lanusse et al. 2017) and by either machine learning methods (e.g., Paraficz et al. 2016; Lanusse et al. 2017) or visual inspection by citizen-science volunteers in Space Warps through the Space Warps project (More et al. 2016) have, between them, discovered an average of four lenses per square degree, so one can be optimistic about finding many thousands of lenses in the next generation of wide-field surveys, from the LSST in optical and the ground-based surveys such as LSST in the optical window and SKA in radio on the ground, and, to space-based missions such as Euclid and WFIRST in orbit.

The expected flood of new lens discoveries will need a similarly huge equally large modelling effort to reconstruct their mass distributions. To prepare for the challenge of massive-sample lens modelling, Küng et al. (2015) developed a new modelling strategy, implemented as the SpaghettiLens system. The idea is to collaborate with experienced members of the citizen-science community, who have already participated in lens discovery—the discovery of gravitational lenses through Space Warps, as well as in several other projects involving astronomical data. The system was tested on a sample of simulated lenses, which that were part of the training and testing set in Space Warps.

This paper continues follows up that study by applying SpaghettiLens to lens candidates discovered through Space Warps candidates discovered through Space Warps. We present results from the modelling of 58 of the 59 lens candidates reported by More et al. (2016). Each lens candidate was modelled in following a collaborative refinement process, where anyone interested can create a new model or modify could improve the analysis by modifying an existing model to try and make it better.<sup>1</sup>

<sup>1</sup> This is in contrast to the main Space Warps project for discovering lenses, where volunteers in a crowd of  $\gtrsim 10^4$  make independent contributions. Each person is presented with a random selection of survey patches and invited to (in effect) vote on each. The system estimates each volunteer’s skill level according to test-patches interspersed with the real data, and weights their votes accordingly (Marshall et al. 2016). There is an active forum for volunteers, but since everyone is seeing different

The or creating a new one. Note the difference with respect to the 2005 main Space Warps project, where volunteers from Springel et al. (2006) people make independent contributions. Each person is presented with a random selection of survey-patches and invited to (in effect) vote on each. The system estimates the skill level of each volunteer according to test-patches interspersed with the real data, and weights their votes accordingly (Marshall et al. 2016). There is an active forum for volunteers, but since everyone is seeing different data samples with minimal overlap, the forum has little if any influence on the result. Please make sure the following is correct: In SpaghettiLens, the number of volunteers is significantly lower, but the level of interaction is higher. The resulting model represents a consensus among contributors, as to the best that could be achieved with the available data and software.

**Interpretation** We emphasize that the interpretation of the results presented here is tentative, because the systems are lens candidates at this stage, not secure lenses. Moreover the candidate-lens redshifts have large uncertainties, while the candidate-source redshifts can only be guessed at present. Nevertheless it is interesting to see what trends we can observe with the already available explore the trends observed with the already available data.

This paper is organized as follows: Section 2 introduces the candidates, the candidate lenses, their models and the diagnostics applied to them. The following sections elaborate on the diagnostics. Image morphology diagnostics are explained in Section 3 and diagnostics based on the mass models are discussed in Section 4. Stellar masses are calculated presented in Section 5, to compare stellar to lensing masses of the candidates. Section and lensing masses. Finally, section 6 summarises and tabulates the diagnostics in Table 1.

**There are** We include three appendices devoted to various technical issues relating to the modelling. The online supplement gives results for the results from all the modelled systems generated for all the lensing candidates.

## 2 THE CANDIDATES AND MODELS

Space Warps is a citizen science gravitational lens search (Marshall et al. 2016). Its first run searched the CFHT Legacy Survey, a survey carried out in five optical bands ( $u^*, g^*, r^*, i^*, z^*$ ) covering a total area of  $160 \text{ deg}^2$  divided up into four fields W1 – W4. It—The MegaPrime camera, used for the survey, has a field of view of  $1 \text{ deg}^2$ , a pixel size of  $0.186''$  and the deepest limiting magnitude is  $25.47$  in the  $g$ -band (Gwyn 2012)<sup>2</sup> pixels. The flux limit of the survey is  $g' < 25.6 \text{ AB}$  ( $5\sigma$ ) with a typical seeing FWHM  $\sim 0.7''$  (Erben et al. 2013). The cutouts shown to the volunteers were colour composites of the  $g$ ,  $r$  and  $i$  band of  $g'$ ,  $r'$  and  $i'$  bands from randomly chosen regions. It—The programme (More et al. 2016) resulted in 59 new lens candidates (of which 29 promising) lens candidates that have not been found by other searches already and in the rediscovery of are promising

data samples with minimal overlap, the forum has little if any influence on votes.

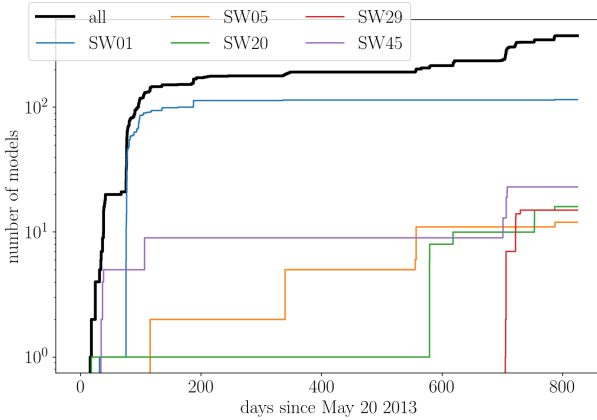


**Figure 1.** Number of models generated over time in days since the launch of SpaghettiLens; the black line shows all models, the coloured lines show the five most active candidates. A total of 377 models were generated for 58 lens candidates, eight users contributed more than five models per person.

#### IF: why are they promising? explain this here).

Moreover, 82 previously known lens candidates were “rediscovered”. The candidates have broadly similar redshifts ( $0.2 < z < 1.0$ ), Einstein radii (between 0.7 and 5”), and arc magnitudes (between 22 and 26) as IF: in the  $g'$  band? These properties are similar to those found by previous robotic searches like ArcFinder and RingFinder (More et al. 2016).

A first version of SpaghettiLens<sup>1</sup> was launched in May 2013, while the first run of Space Warps was ongoing. Figure Fig. 1 shows the total number of models generated since launch, but only includes models for the for our lens candidates. A small number of volunteers started to work with to create creating models of possible lens candidates found in from Space Warps that were debated on in the discussion forums in the discussion forum. In the beginning of August 2013 (around day 70 since release) a modelling challenge for the candidate later to be identified as SW01 was launched. A group of five volunteers converged to a set of favourite models that they presented presented their results in an online letter after REFERENCE? about 65 days passed and later converging on a set of 30 models have been created for this particular system. In April 2015 (day 700), the first major release version of SpaghettiLens was presented. In released. At the same time, the list of identified candidates was made available (as a preprint of More et al. 2016). At this stage, the volunteers were asked to create models for all the lens candidates that were still missing. The generated models work done for candidate SW29 show that the volunteers converged to on a favourable model much faster, after 15 models generated in 30 days.

This The total modelling effort resulted in a total set of 377 SpaghettiLens models for all but one of the 59 Space Warps lens candidates; candidate SW39 was not modelled by any volunteer. Over its runtime the system saw, the system logged eight major contributors (volunteers that

at least generated five models each defined as volunteers that generated, at least, five models).

In parallel Künig et al. (2015), Künig et al. (2015) tested the system on simulated lenses and identified some areas for improvement. In § A1 we introduce fitting of the brightness profiles surface brightness profile of the source. This feature has not yet been included been included yet in SpaghettiLens, but has been carried out in we carried the analysis during post-processing for a few especially interesting candidates interesting cases. In § A2 we show that making mass maps fine-grained in fine-grained mass maps within the central region relieves a tendency in the earlier work for mass profile profiles to be too shallow. Then in In § A3 we consider the possibility of fitting a parametric lens model to the model ensemble; so far we have only been successful at extracting an Einstein radius ensemble.

We characterise each model with seven diagnostics, grouped into three categories, whose purpose is to help identify which systems are most probably lenses, and which ones are likely to be most rewarding the most likely cases of a gravitational lens, as well as flag the most interesting candidates for future follow-up observations. The diagnostics are as follows.

- First Firstly we have diagnostics based on morphology of the system. Section 3 and Figure Fig. 2 explain –this diagnostic in more detail. We consider:

- (i) Whether the images are unblended. Distinct: Distinct, unblended images are an advantage in modelling, but although not essential.
- (ii) Whether all images are discernible. The topography of an arrival-time surface, as encoded by a spaghetti diagram, may require more images than are visible, in which case the modeller has to insert conjectural image positions.
- (iii) Whether the lens is fairly isolated.
- (iv) The image morphology concisely described: double or quads, further sub-categorised to indicate the elongation direction of the lensing mass.

- Second Secondly we have mass models, covered in Section 4. We assess the following points:

- (v) Whether the mass map is reasonable (see Fig. 5). Figure 5–
- (vi) Whether the arrival-time surface and synthetic image are plausible. In particular, an unsatisfactory model is flagged when additional images are implied in regions where they are not observed signal an unsatisfactory model. Figures 3 and 4 and 6 (see Figs. 3, 4 6).

- Third Thirdly, whether the total implied lensing mass determined from the lens model is plausible, given the photometry of the lensing galaxy. In this work we define the lensing mass as the sum of all mass tiles needed to model lens in the model. These mass tiles reach out to typically twice the radius of the the outermost image. Section 5 explains how we compare the lensing mass with the mass in stars in the lensing galaxy. We estimate the stellar mass by comparing galaxy magnitudes from the CFHTLS pipeline with the well-known stellar population models of Bruzual & Charlot (2003). We then extrapolate the stellar mass to a halo mass using the abundance matching prescription of Moster et al. (2010) (i.e.

<sup>1</sup> IF include web link: <http://xxx.yyy.ch>

total) mass with the stellar mass. Naturally, the lensing mass must be more than should be somewhere between the stellar mass but no more than (lower bound) and the total halo mass (upper bound).

(vii) We then introduce what we call a a so-called halo index ( $H$ ) which gives an idea of that quantifies how the lensing mass compares with these two constraints (see Fig. 7). Figure 7.

### 3 IMAGE MORPHOLOGY

A modeller's main input to the lens-modelling The main input of a modeller to the process is a markup of the candidate lens system, which we call a spaghetti diagram. This is a sketch of the arrival-time surface from a point-like source, with proposed locations of maxima, minima and saddle points, and an implied time-ordering of the images. Such information encodes a starting proposal for the mass distribution. A spaghetti diagram is thus a completely abstract construction, and moreover it refers to a simplified system with a point source. However, spaghetti diagrams are intuitive because they tend to resemble the form of lensed arcs (see fig. 3 of Ferreras et al. 2008), and of course they are simple to draw, and easy to vary and refine in an open collaborative environment. This makes them very practical for non-professional lens enthusiasts in the citizen-science community. Details and tests are given in Küng et al. (2015) Kung et al. (2015).

We now discuss the diagnostics that can be taken from the process of drawing the spaghetti diagram, even before detailed mass-modelling takes place. Figure Fig. 2 shows nine examples, each consisting of a cutout of the Space Warps Space Warps image of a lens candidate, marked up with a spaghetti diagram. The volunteers are initially presented the original Space Warps image of length and height a square image with side 82'' (440 pixels) in full size, but they have the ability to zoom in individually. The cutouts presented in Figures Figs. 2 to 5 are rescaled in during post-processing, relative to the outermost image identified.

All the examples in Figures shown in Fig. 2 identify five locations: the centre of the main lensing galaxy, which is also a maximum of the arrival time surface (red dots); two minima (blue dots); and two saddle points (green dots and also self-intersections of the curves). Only two (SW05 and SW42) of the nine systems, however, have five distinct features in plausible locations. In the other seven examples, an arc is interpreted as a blend of three or four images. This gives defines the 'unblended images' diagnostic. Note that this characterisation could be different if the spaghetti diagram is were different. For example, SW28 has also been modelled with the arc on the right interpreted as a single image, rather than as three images as shown in the figure; for such a model, the 'unblended images' diagnostic would be true.

The second diagnostic is checks whether all images are visible. For example, we see in SW58 at the top left of Figure Fig. 2 that an image at the second minimum is conjectural and does not correspond to any visible feature.

The third diagnostic is tests whether the lens is fairly isolated, or whether there are other galaxies in the field that probably contribute significantly other galaxies could contribute to the lensing. For this, we do not consider stars

or other clearly foreground objects. Additional galaxies contributing to the lensing mass can be marked by the volunteer alongside the spaghetti diagrams. An example can be seen as the grey dot and circle in the cutout with SW57 at the top right of Figure Fig. 2. Objects marked in this way are modelled as point masses. Other possible contributors to lensing are galaxies or groups that are not in the immediate vicinity of the lensed images, yet massive enough to have an effect exert an influence. These are accounted for by allowing a constant but adjustable external shear.

We remark that blended images or missing the lack of expected lensed images, or the presence of blended images or perturbing galaxies do not imply that a given candidate is unlikely to be a lens. They mean This means, rather, that the models are more uncertain and perhaps could be more easily improved by trying further variations in the markup.

The fourth diagnostic is based on the fact that the arrangement of lensed images of a pointlike source through a non-circular gravitational lens depends on the location of the source relative to the long and short axes of the lens. This dependence is quite robust and independent of many other details of the lensing mass distribution. Sources close to being dead-centre behind a lens tend to produce quads, sources at larger transverse distance tend to produce doubles. We denote these as Q and D, respectively, and add a prefix to the Q systems, as follows: we write LQ if the source is inferred as displaced along the long axis of the lens, SQ if displaced along the short axis, IQ if inclined to both axes, CQ if only very little to no displacement or no displacement is evident. Although the unlensed source and its location are obviously not seen, the LQ, SQ, IQ and CQ cases correspond to easily-seen image morphologies (see, e.g., Saha & Williams 2003).

- The simplest is the SQ case: this creates a saddle point and two minima in an arc, with the second saddle point on the other side of the lensing galaxy, and at a closer to the galaxy than the arc is. SW58 and SW28 in the upper row of Figure Fig. 2 are typical examples of SQ. If the source would move were moved outwards along the short axis, the minimum-saddle-minimum set would merge into a single minimum, leaving a D system; the transition is known as a cusp catastrophe.

- The middle row of Figure Fig. 2 shows three IQ systems, SW05, SW42 and SW19. This type has a characteristic asymmetry, often with two images close together. If the source would move were moved outwards, the minimum-saddle pair would merge and mutually cancel, again leaving again a D system; the. This transition is known as a fold catastrophe.

- The lower row of Figure Fig. 2 shows three LQ systems, SW09, SW29 and SW02, and the failed model. The failed model, SW57, at top right also possibly belonging may also belong to this category. Here the images have a fairly symmetric arrangement with an arc and a counter-image on the other side, but the spaghetti diagram is completely asymmetric. If the source would move were moved outwards along the long axis, the saddle-minimum-saddle set would merge into a single saddle — another form of cusp catastrophe. LQ can be visually distinguished from SQ from by the relative distances of the arc and the counter-image. For LQ the arc is closer, for SQ the counter-image is closer.

CQ systems are often called ‘cross’ or ‘Einstein-cross’ systems; IQ systems are sometimes called ‘folds’, with ‘cusp’ commonly used for both SQ and LQ. The labels ‘short-axis quad’ and so on are not standard in the literature, but the morphological classification they express is familiar to experienced modellers. Hence they can be useful to researchers wishing to apply other modelling methods to the same systems.

#### 4 MASS MODELS

Once a spaghetti diagram has been drawn on a web browser, it is forwarded to a server-side numerical framework, which searches for mass maps consistent with the given image locations, parities and time ordering given by the modeller. The mass maps are made up of mass tiles and are free-form, but are required to be concentrated around the identified lens centre (see Coles et al. 2014, for the precise formulation of the search). Assuming such mass distributions can be found (which in practice is usually the case) a statistical ensemble of two-dimensional mass maps is returned. This ensemble, along with derived quantities and uncertainties, makes up one SpaghettiLens model.

The mass will naturally depend on the lens and source redshifts, which are unknown when a lens candidate is first identified. But However, this is not a problem, because a model can be trivially rescaled to use better redshift values, as and when they become available. This work applies photometric redshifts from the CFHTLS pipeline (Coupon et al. 2009) to the candidate lensing galaxies; the values range from  $z=0.2$  to  $z=1$  (see Table 1). These redshifts entail rather big uncertainties, up to a few ten percent. Since however, the angular critical density is proportional to  $d_L d_s d_{ls}^{-1}$  (consult Equation A1 in Küng et al. 2015) it is neglectable-negligible for this tentative analysis.

**IF:** I would not say this is “negligible” but, rather, that As the mass normalisation depends only weakly on the source redshift, provided it is larger higher than the lens redshift, we assumed all sources lie at  $z=2$  adopted a redshift  $z=2$  for all sources unless an unambiguous photometric redshift is available.

**IF:** Again, a simple quantification of the change you expect

The ensemble of mass maps can be post-processed in many different ways. Four different graphical quantities are particularly useful.

FigureFig. 3 shows the arrival-time surfaces corresponding to the spaghetti diagrams in FigureFig. 2. The arrival-time contours look like machine-made elaborations of the input spaghetti diagrams. If the saddle-point contours in the arrival time are qualitatively the same as the curves in the spaghetti diagram (the detailed shape of the spaghetti curves is unimportant), it immediately suggests a successful model. On the other hand, if the arrival-time surface has unexpected minima or saddle points, and especially if the unexpected features are far from identified lens images, that signals a doubtful model. FigureFig. 4 shows what we call synthetic images, meaning reconstructions of the extended lensed features by fitting for a source. These were generated by a new method, explained in Appendix A1, implemented during the offline post-processing after the

modelling process was complete. The synthetic images provided by SpaghettiLens during the collaborative modelling and discussion were more crude; these those are included in the online supplement.

The arrival-time surface and synthetic image are summarised by one diagnostic, the most important of all: are the lensed features satisfactorily reproduced? This diagnostic remains a judgment call by modellers. A useful quantitative criterion for whether the synthetic image is consistent with the data would need to allow for PSF dependence and unmodelled substructure —otherwise— otherwise all models would be summarily rejected —and it is not clear how to do this rejected, something left for a future implementation in SpaghettiLens.

FigureFig. 5 shows the projected mass maps of the example systems. Actually sample, In fact, this figure only shows the ensemble-average mass maps, and not the variation with the Galaxies 2 filaments which project finite claim of the search inferred. (The same applies to the arrival-time surfaces and synthetic images in the two previous figures. Uncertainties previous two figures. The uncertainties will be shown in a concise form later, with FigureFig. 6.) FigureFig. 5 makes evident the tiled nature of the mass model. The tiles can be smoothed over by interpolation, and this was actually done in the mass maps shown online during the modelling process, available in the online version. It is interesting, however, to see note the tiling artifacts, if only as a reminder that the substructure in the mass distribution are is very uncertain, even if some integrated quantities are very well constrained. How the free-form mass maps relate to parameterised lens models is discussed in Appendix A3. Note that the arrival-time surface does not have discontinuous jumps, because the modelling numerics uses an analytical integral over square tiles; likewise the lens equation.

**IF:** This sentence is confusing and needs some clarification: No the error in the redshift would lead to surface mass density un

FigureFig. 6 shows the enclosed-mass profiles, expressed as the average convergence  $\kappa$ , within circles of given projected radius. This time, uncertainties The uncertainties IF: at the BLAH level are included. Appendix A2 describes the improvements made since our earlier work (Küng et al. 2013), to allow for steeper profiles in the inner regions.

The enclosed mass is typically best constrained at the national Einstein radius, becoming more uncertain at larger and smaller radii.

The mass maps and mass profiles are the basis of a further diagnostic: are the mass distributions plausible? This again is is also a judgment call made by modellers, but it showed to be a powerful diagnostic, summarizing three aspects. Usually the The overall shape is forced to be 180°-rotation symmetric and turns out plausible usually a plausible assumption, but volunteers can deactivate this constraint. The profile slope turned out to be a good indicator for of plausible models, as can be seen by comparing the contrasting model SW 57 to others with the rest of the sample: The missing core in FigureFig. 5 and the flat profile in FigureFig. 6 disqualify this model. The clumpiness of the mass map is another one useful indicator. Flat profile slopes can often be identified directly in the mass map, where the mass tiles form a checkerboard pattern.

## 5 STELLAR AND HALO MASS ESTIMATES

The stellar masses of the lens galaxies are derived by comparison of the photometric data with *stellar* M/L estimates from population synthesis models. In principle, a detailed analysis of the spectral energy distribution is needed to derive accurate stellar masses (e.g. Gallazzi & Bell 2009; Taylor et al. 2011). However, estimates to within  $\approx 0.3$  dex in  $\log(M_{\text{stel}}/M_{\odot})$  can be derived with a single colour, preferably tracing a rest-frame colour similar to  $U - V$  (see Fig. 1 of Ferreras et al. 2008), assuming a universal initial mass function (IMF). There is some evidence from spectral lines evidence from detailed absorption line strength analysis that massive galaxies tend to have a more bottom-heavy IMF than the Milky Way, but a much higher stellar mass-to-light would over-predict the mass in some lensing systems (Smith et al. 2015b) can feature a non-standard IMF (e.g. Ferreras et al. 2013). However, these variations – towards a bottom-heavy distribution – are typically found in the cores of massive early-type galaxies (La Barbera et al. 2016). The effect of these variations on the stellar M/L of lensing systems is still rather controversial (Smith et al. 2015a; Leier et al. 2016).

In this paper we further simplify the analysis by assuming a relationship between the apparent total magnitude and stellar mass, at the redshift of the lens. For typical stellar-population parameters, the variation of this relation is at most  $\Delta \log M_s \sim 1$  dex. A further possible systematic error is potential systematic can arise from contamination of the light of the lensing galaxy by the lensed background galaxy source. Reducing or eliminating the latter would require detailed fitting of light distributions for each candidate (see Leier et al. 2011), which we have not yet attempted. Nonetheless, because the lensing masses range over two orders of magnitude, it is still interesting to compare with very rough stellar masses them with rough estimates of stellar mass.

We make use of the Bruzual & Charlot (2003) models to derive two functional forms of the stellar mass with respect to SDSS-*i*-band the *i'*-band magnitudes. The models have solar metallicity, with a Chabrier IMF, and assume two different age trends: a “young” model, with a constant 500 Myr age at all redshifts, and an “old” model where the age is the oldest one possible at each redshift, adopting a standard  $\Lambda$ CDM model with  $H_0 = 70 \text{ km s}^{-1} \text{ Mpc}^{-1}$  and  $\Omega_m = 0.3$ .

**Figure** Fig. 7 shows a comparison of stellar and lensing masses mass in our sample. The comparatively large span in the stellar mass of the error bars in stellar mass (horizontal axis) shows the range between the masses derived using the two age trends respectively, and lies between 0.4 and 0.8 dex. It will be improved in future work by using the use of available optical and NIR magnitudes to derive more accurate constraints on the stellar populations. In addition, we also derive halo masses for the lenses using an abundance-matching formula. This technique matches the distribution function of observed stellar mass in galaxies with that of dark-halo masses in from N-body simulations to derive to define a simple relation between stellar mass and halo mass. We emphasize that a halo mass from abundance matching should be considered an “average” estimate, and a significant scatter can be expected as galaxies with the same stellar mass can be found in different environments. We refer the

reader to Leier et al. (2012) for an assessment of the effect of abundance matching on the derivation of dark matter halo properties in lensing galaxies. We follow the prescription of Moster et al. (2010), namely:

$$\frac{M_{\text{stel}}}{M_{\text{halo}}} = \frac{2C_0}{(M_{\text{halo}}/M_1)^{-\beta} + (M_{\text{halo}}/M_1)^{\gamma}} \quad C_0 = 0.02820, M_1 = 10^{11.884} M_{\odot} \quad \beta = 1.057, \gamma = 0.556 \quad (1)$$

**Figure**

$$C_0 = 0.02820, \quad M_1 = 10^{11.884} M_{\odot} \\ \beta = 1.057, \quad \gamma = 0.556.$$

Fig. 7 may be compared with Figure fig. 4 in More et al. (2011).

The comparison of lensing and stellar masses provides us with mass produces the last of our model diagnostics. This is defined as a halo-matching index:

$$\mathcal{H} \equiv \frac{\ln(M/M_{\text{stel}})}{\ln(M_{\text{halo}}/M_{\text{stel}})} \quad (2)$$

that relates the observed lensing to stellar mass, with the global ratio expected if the host halo corresponds to the average value derived by abundance matching. Several cases for  $\mathcal{H}$  can be considered:

- $\mathcal{H} < 0$  is unphysical because  $M < M_{\text{stel}}$ .
- $\mathcal{H} = 0$  is when means the stellar mass exactly accounts for the lensing mass (i.e. no dark matter affects the lensing model).
- $0 < \mathcal{H} < 1$  is the typical situation, where the lens includes stars and dark matter, but not the full halo.
- $\mathcal{H} = 1$  means that the lens consists of the entire halo.
- $\mathcal{H} > 1$  is in tension with abundance-matching, because the lensing mass exceeds the expected halo mass.

The halo-matching index expresses whether the lensing mass is plausible given the light flux received from the candidate lensing galaxy.

Figure Fig. 7 and Table 1 show that most of the candidates having have stellar and lensing mass masses typical of massive ellipticals<sup>2</sup>. SW05 is one of the most massive of all the candidates, with a mass of corresponding to a galaxy-group mass scale. It is a particularly attractive system for follow-up observations at higher resolution, as it is a large system with clear multiple-image features, and modelling. Modelling leaves little doubt that it is a lens. SW04 seems to be even more massive, but the diagnostics leave some doubts about the validity of this model. The two lowest-mass systems, SW19 and SW42, are important if they are indeed lenses, as they would be low-mass lenses dominated by dark matter. All the modelled systems have reasonable stellar-mass fractions, except for two cases where the stellar-mass fraction is too low ( $\mathcal{H} > 1$ ): these are SW42 and SW57. In the case of SW57, the model has poor diagnostics and should be discounted discarded. The model for SW42, on the other hand, is quite convincing — except for the high halo-matching index. If SW42 turns turned out not to be a lens, that would support the halo-matching index as an effective criterion for filtering to discriminate models.

<sup>2</sup> Exact values can be found in the online version of Table 1

## 6 SUMMARY AND CONCLUSIONS

We report on a first set of mass distributions and ~~follow-up~~ diagnostics for the Space Warps lens candidates created with a novel approach that aims to be scalable by ~~orders of magnitudes~~ ~~orders of magnitude~~ to prepare for the many thousands of lenses the next generation of wide field surveys will yield – (e.g. Euclid, WFIRST).

The Over the past few years, the way of discovering lenses ~~is changing has changed~~ with the introduction of machine learning and citizen science ~~methods~~, combined with the coverage of ~~huge areas large areas of the sky~~ by modern surveys. The way ~~lensing~~ mass models are constructed also needs to change, in order to be prepared for the increasing influx of ~~lenses to be modelled~~. This work is a hybrid of ~~lens candidates~~. The work in this paper represents a hybrid approach between the classical style – where a small team of experts invest many hours into the creation of a single model, ~~with the approach of citizen science~~, and a citizen science project – where a crowd of amateur volunteers make independent contributions. We ~~The authors of this paper~~ are a collaboration of ~~professionals professional~~ and experienced citizen-science volunteers, aiming to create early-stage lens models as soon as a lens candidate is found.

To ~~assists volunteer modellers assessing their assist~~ volunteers in constraining lensing models, we introduce a set of diagnostics ~~allowing the qualification of the lenses and the generated models and present them alongside the generated models that help asses the validity of the models~~. At a later stage, we encourage modellers to apply those diagnostics ~~themselves to get a preliminary as~~ feedback on the plausibility of their ~~models and possibly assumptions~~, and to suggest additional diagnostics.

The diagnostics (i) – (iv) (see Section 2) turned out to be useful ~~for evaluating how difficult a system is to model~~ measures of the difficulty in modelling a system, but they ~~weren't did not constitute~~ necessary conditions for a promising model. They can help select systems to ~~present to introduce~~ novice volunteers to ~~introduce them to~~ the modelling process. Diagnostics In contrast, diagnostics (v) and (vi) ~~on the other hand~~ can be considered as necessary criteria for a good model. Volunteers employed those ~~ones~~ to evaluate their models ~~and they~~, and turned out to be easy enough to grasp ~~for by~~ new volunteers. The halo-matching index  $\mathcal{H}$ , diagnostic (vii)  $\mathcal{H}$ , is an interesting criterion that might be useful for ~~volunteers the modellers~~, but needs further investigation ~~to be established~~.

Table 1 is a summary of our results. It characterises each modelled system with seven diagnostics, indicating (a) the image morphology and how clear or indistinct it is, (b) whether the mass map and synthetic lensed image appear to be plausible, and (c) how the model mass compares with the estimated stellar and full-halo masses. Missing entries are due to ~~photometry data not being available~~ unavailable imaging data, whereas missing rows are due to models ~~not having been that were not~~ created for this particular candidate.

The trend in Figure Fig. 7, ~~that where~~ higher-mass galaxies get progressively more dark-matter dominated, is expected, e.g. see Ferreras et al. (2005), (see, e.g. Ferreras et al. 2005), as is the span of about one order of magnitude for the stellar mass and the two ~~order of magnitudes for the orders of magnitude in~~ lensing mass.

With future data, it ~~would will~~ be interesting to compare ~~the~~ enclosed stellar and lensing mass as a function of radius, going from ~~the~~ star-dominated inner regions to ~~the outer~~ dark halos. Leier et al. (2011) Leier et al. (2011) illustrate this behaviour in their Figure fig. 5, but the present sample could go an order of magnitude higher in mass.

The quick creation of many models for the Space Warps candidates successfully showed that a subset of citizen scientists are interested in being involved in more challenging tasks that take some time to learn. A ~~next steps~~ The next step involves recruiting more lensing enthusiasts, as soon as the next round of Space Warps is started. In the meantime, the improvements shown in the Appendix ~~have to been integrated into regular will be integrated in the standard version of SpaghettiLens usage~~. Additionally, photometric fitting could Photometric fitting could also be integrated into SpaghettiLens. This would allow experienced citizen scientists to generate photometric redshifts and stellar masses, and thus generate preliminary dark-matter maps as soon as a lens-candidate is identified.

## REFERENCES

- Bruderer C., Read J. I., Coles J. P., Leier D., Falco E. E., Ferreras I., Saha P., 2016, *MNRAS*, 456, 870  
 Bruzual G., Charlot S., 2003, *MNRAS*, 344, 1000  
 Coles J. P., Read J. I., Saha P., 2014, *MNRAS*, 445, 2181  
 Coupon J., et al., 2009, *A&A*, 500, 981  
 Cuillandre J.-C. J., et al., 2012, in Observatory Operations: Strategies, Processes, and Systems IV. p. 84480M, doi:10.1117/12.925584  
 Erben T., et al., 2013, *MNRAS*, 433, 2545  
 Ferreras I., Saha P., Williams L. L. R., 2005, *ApJ*, 623, L5  
 Ferreras I., Saha P., Burles S., 2008, *MNRAS*, 383, 857  
 Ferreras I., La Barbera F., de la Rosa I. G., Vazdekis A., de Carvalho R. R., Falcón-Barroso J., Ricciardelli E., 2013, *MNRAS*, 429, L15  
 Gallazzi A., Bell E. F., 2009, *ApJS*, 185, 253  
 Gavazzi R., Marshall P. J., Treu T., Sonnenfeld A., 2014, *ApJ*, 785, 144  
 Gwyn S. D. J., 2012, *AJ*, 143, 38  
 Heymans C., et al., 2012, *MNRAS*, 427, 146  
 Keeton C. R., 2001, preprint, ([arXiv:astro-ph/0102341](https://arxiv.org/abs/astro-ph/0102341))  
 Koopmans L. V. E., et al., 2009, *ApJ*, 703, L51  
 Künig R., et al., 2015, *MNRAS*, 447, 2170  
 La Barbera F., Vazdekis A., Ferreras I., Pasquali A., Cappellari M., Martín-Navarro I., Schönebeck F., Falcón-Barroso J., 2016, *MNRAS*, 457, 1468  
 Lanusse F., Ma Q., Li N., Collett T. E., Li C.-L., Ravanbakhsh S., Mandelbaum R., Poczos B., 2017, preprint, ([arXiv:1703.02642](https://arxiv.org/abs/1703.02642))  
 Leier D., Ferreras I., Saha P., Falco E. E., 2011, *ApJ*, 740, 97  
 Leier D., Ferreras I., Saha P., 2012, *MNRAS*, 424, 104  
 Leier D., Ferreras I., Saha P., Charlot S., Bruzual G., La Barbera F., 2016, *MNRAS*, 459, 3677  
 Marshall P. J., et al., 2016, *MNRAS*, 455, 1171  
 Maturi M., Mizera S., Seidel G., 2014, *A&A*, 567, A111  
 McGaugh S. S., Lelli F., Schombert J. M., 2016, *Physical Review Letters*, 117, 201101  
 More A., Jahnke K., More S., Gallazzi A., Bell E. F., Barden M., Häubler B., 2011, *ApJ*, 734, 69  
 More A., Cabanac R., More S., Alard C., Limousin M., Kneib J.-P., Gavazzi R., Motta V., 2012, *ApJ*, 749, 38  
 More A., et al., 2016, *MNRAS*, 455, 1191

- Moster B. P., Somerville R. S., Maulbetsch C., van den Bosch F. C., Macciò A. V., Naab T., Oser L., 2010, *ApJ*, **710**, 903  
Paraficz D., et al., 2016, *A&A*, **592**, A75  
Saha P., Williams L. L. R., 2003, *AJ*, **125**, 2769  
Saxton C. J., Ferreras I., 2010, *MNRAS*, **405**, 77  
Schive H.-Y., Chiueh T., Broadhurst T., Huang K.-W., 2016, *ApJ*, **818**, 89  
Silk J., Mamon G. A., 2012, *Research in Astronomy and Astrophysics*, **12**, 917  
Smith R. J., Lucey J. R., Conroy C., 2015a, *MNRAS*, **449**, 3441  
Smith R. J., Alton P., Lucey J. R., Conroy C., Carter D., 2015b, *MNRAS*, **454**, L71  
Sonnenfeld A., et al., 2017, preprint, ([arXiv:1704.01585](https://arxiv.org/abs/1704.01585))  
Springel V., et al., 2005, *Nature*, **435**, 629  
Taylor E. N., et al., 2011, *MNRAS*, **418**, 1587

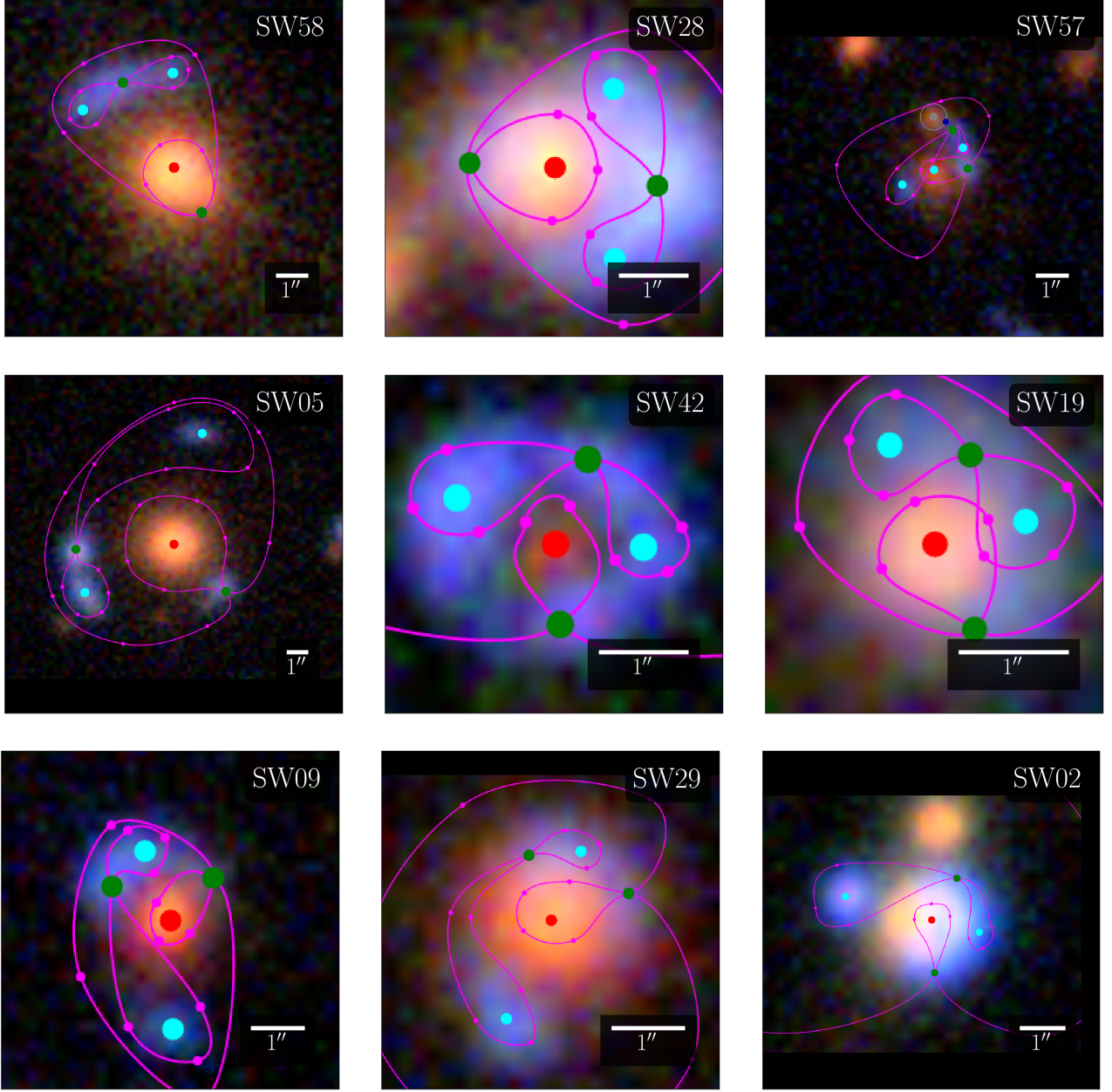


**Figure 2.** Nine of the lens candidates marked up with spaghetti diagrams. Red, blue and green dots are proposed locations for maxima, minima and saddle points of the arrival time respectively. The curves help guide the placement of the dots, but their precise appearance has no significance. These images are screenshots from the SpaghettiLens user interface, which applies interpolation to background images. The scaling is adjusted to fit the other images. This selection includes the best-modelled systems, but also one case (SW57 at upper right) of unsuccessful modelling. Since the modelling process is collaborative among the volunteers, with anyone welcome to contribute new models or modify existing ones, there are variant spaghetti diagrams for all the modelled systems. The online supplement displays all the models presented for discussion during this work.

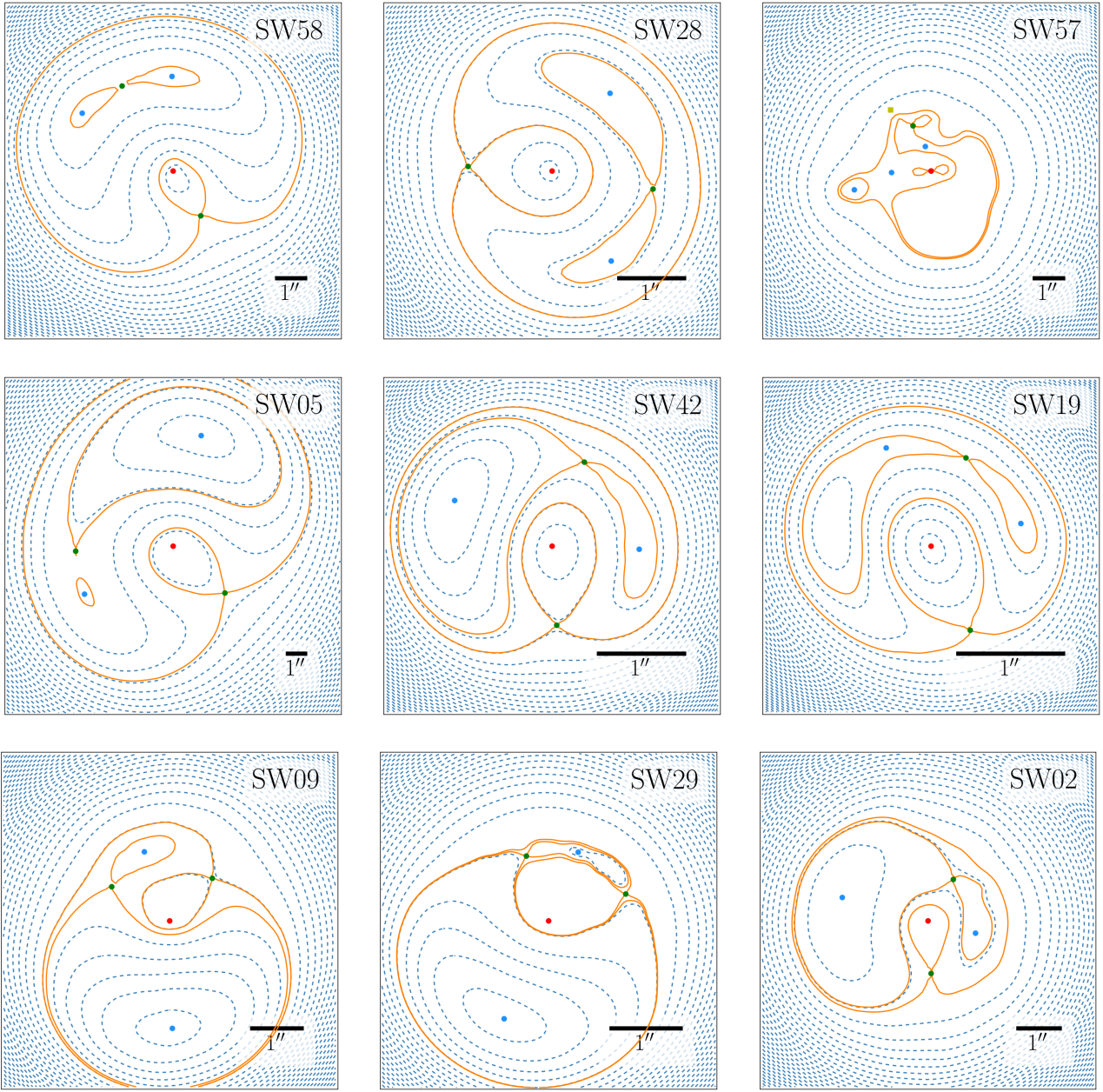


**Figure 3.** Arrival-time surfaces for models of the systems from Figure 2. The registration differs slightly from Figure 2, but the coloured dots represent exactly the sky positions specified in the earlier figure. The orange contours only qualitatively resemble the earlier pink curves, as they are now precise saddle-point contours from lens models.

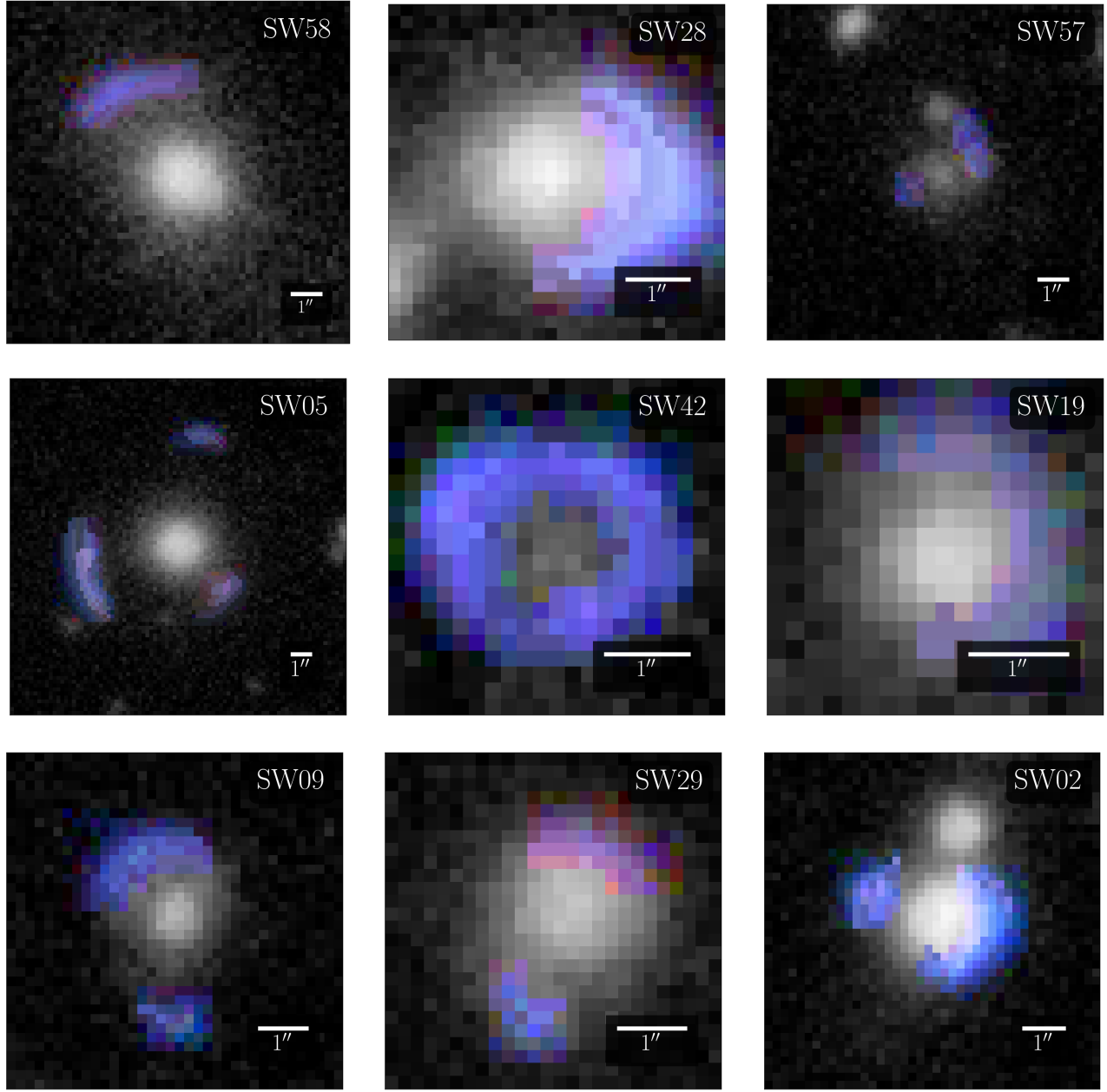


**Figure 4.** Synthetic images of the systems from Figure 2, derived from the lens models. The reconstructed lensed features keep the Space Warps false-colour scheme from Figures 2. The rest has been changed to black-and-white.

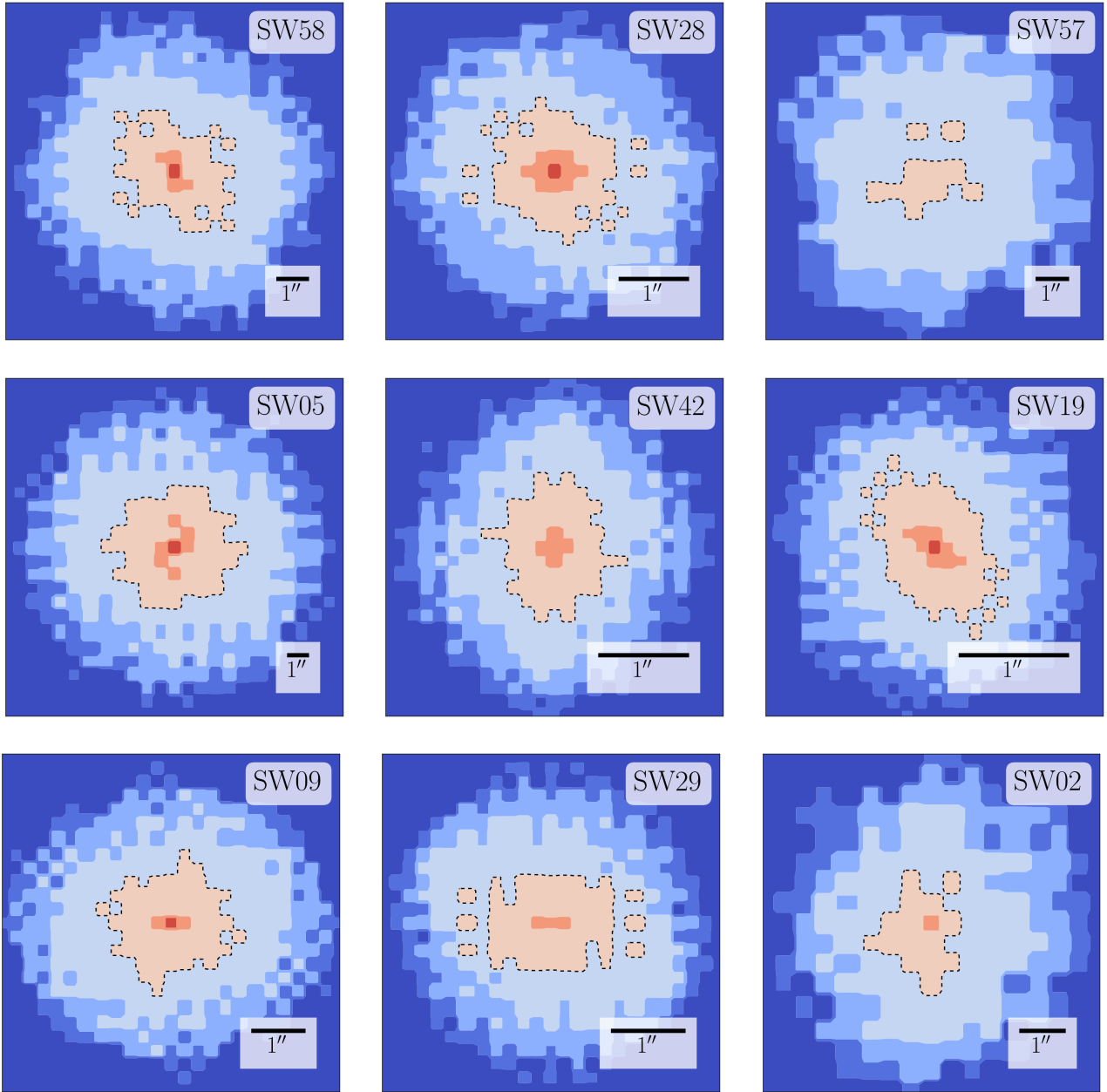


**Figure 5.** Ensemble-average mass distribution  $\kappa$  for which the results Figures 3–4 were derived. The dashed curves denote  $\kappa = 1$ . Most of the mass maps have a  $180^\circ$ -rotation symmetry, which is imposed by default. For SW02 and SW57, where the lensing mass is clearly asymmetric, the modeller chose to turn off the symmetry.

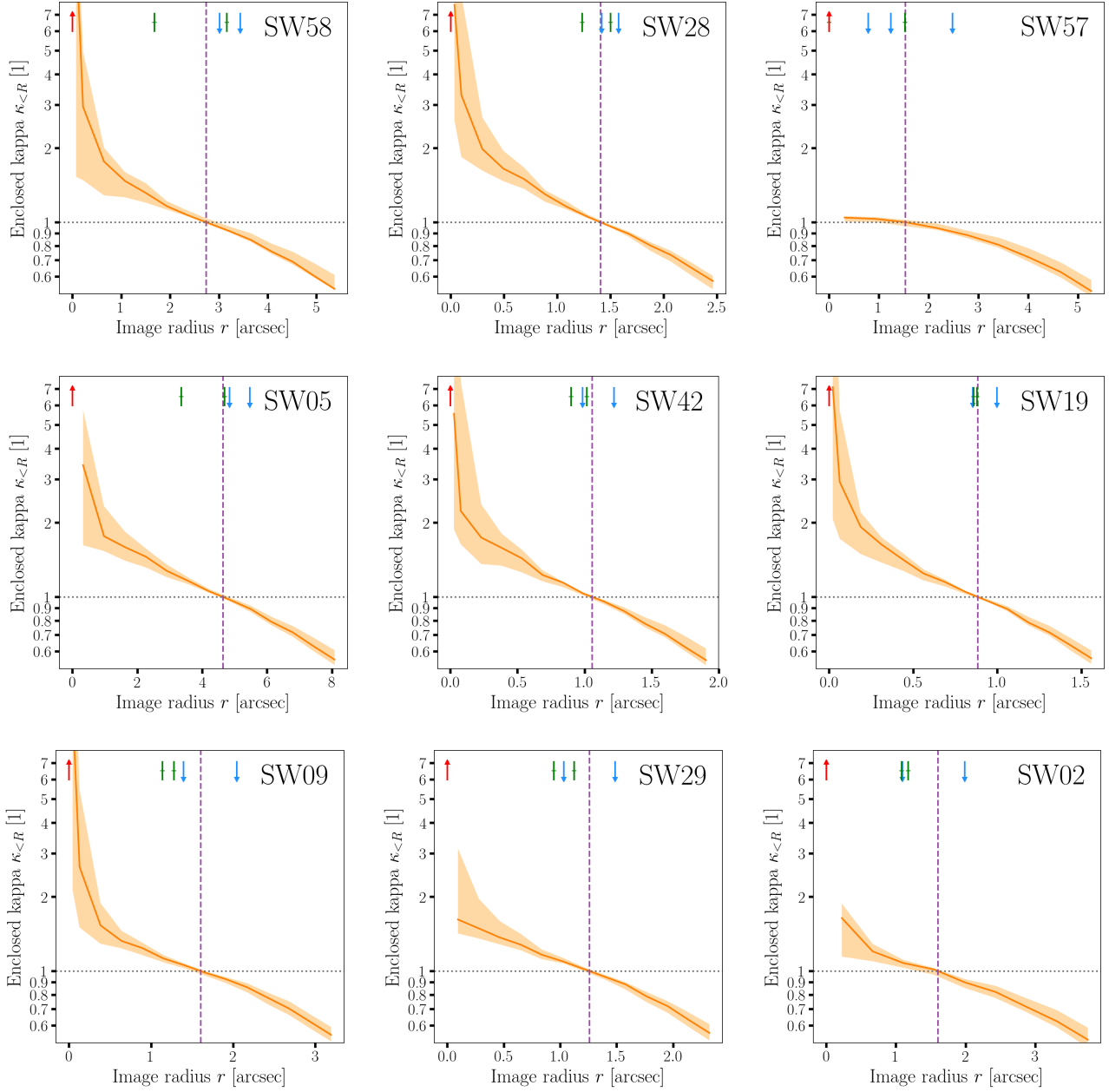


**Figure 6.** Cumulative circular-averages of the mass maps from Figure 5, with uncertainties. More precisely, we show the enclosed mass within a given projected radius, expressed as the mean  $\kappa$  with a given number of arcsec from the centre of the lensing galaxy. The orange bands refer to the full ensemble of mass maps for the models, while the red curves show the ensemble averages. The dashed vertical line indicates the notional Einstein radius, or where the mean enclosed  $\kappa$  is unity. The short vertical arrows marks the positions of the images (maxima, saddle points and minima).

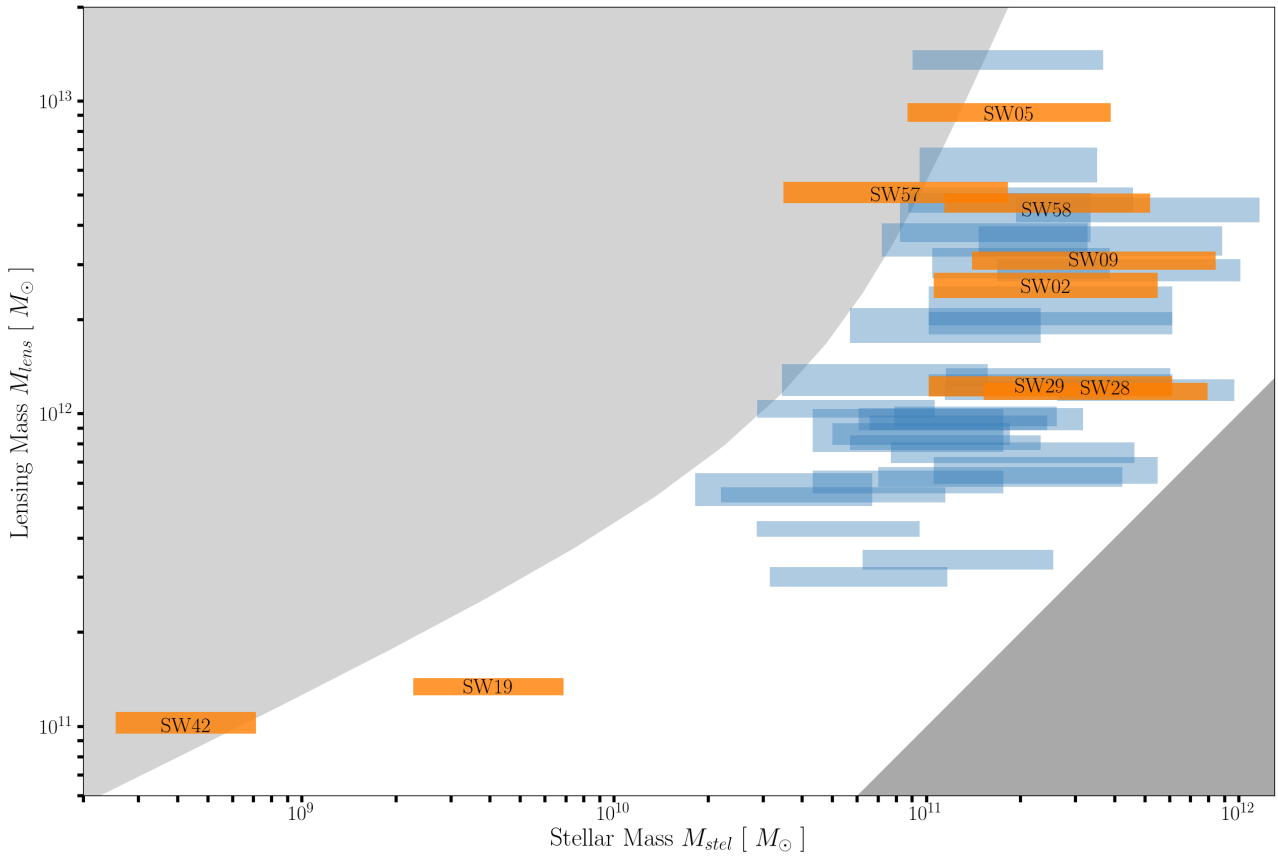


**Figure 7.** Total mass in the model against the estimated stellar mass, alongside the values for the whole sample. (The labelled orange bars are the systems shown in detail in Figures 2–6.) The horizontal extent of each bar indicates the extreme cases of a young (0.5 Gyr-old) stellar population and the oldest possible population at the given redshift. The vertical extent indicates the spread of masses in the lens-model ensemble. The lower-right shaded region is unphysical according to the stellar-population models, because it gives  $M < M_{\text{stel}}$ . The upper-left shaded region is unphysical according to abundance matching (see Section 5) because it gives  $M > M_{\text{halo}}$ . That is to say, the unshaded region is  $0 < \mathcal{H} < 1$ .

**Table 1.** Diagnostics of a selected model for each Space Warps candidate (see Section 6). [Machine-readable](#) A machine-readable version is available in the online supplement.

SWID	ZooID	CFHTLS Name	$z_{\text{lens}}$	unblended images	all images discernible	isolated lens	image morphology	synthetic image reasonable	mass map reasonable	$\log_{10} \frac{M_{\text{stel}}}{M_{\odot}}$	$\log_{10} \frac{M_{\text{lens}}}{M_{\odot}}$	halo-matching index $\mathcal{H}$
SW01	ASW0004dv8	J022409.5–105807	–	✗	✗	✗	SQ	✓	✓	–	–	–
SW02	ASW000619d	J140522.2+574333	0.7	✗	✓	✗	LQ	✓	✓	11.4	12.4	0.47
SW03	ASW0006mea	J142603.2+511421	–	✓	✗	✗	D	✓	✓	–	–	–
SW04	ASW0009cjs	J142934.2+562541	0.5	✓	✗	✗	CQ	✗	✓	11.3	13.1	0.93
SW05	ASW0007k4r	J143454.4+522850	0.58	✓	✓	✓	IQ	✓	✓	11.3	13.0	0.83
SW06	ASW0008swn	J143627.9+563832	0.5	✗	✓	✓	✓	✓	✗	11.1	11.9	0.46
SW07	ASW0007e08	J220256.8+023432	–	✓	✓	✗	D	✓	✓	–	–	–
SW08	ASW0009qed	J020648.0–065639	0.8	✓	✓	✓	D	✓	✓	11.4	12.3	0.40
SW09	ASW0002asp	J020832.1–043315	1.0	✗	✓	✓	✓	✓	✓	11.5	12.5	0.40
SW10	ASW0002bmc	J020848.2–042427	0.8	✓	✗	✗	D	✗	✗	11.3	11.9	0.29
SW11	ASW0002qtn	J020849.8–050429	0.8	✗	✓	✗	LQ	✓	✓	11.2	11.8	0.29
SW12	ASW0003wsu	J022406.1–062846	0.4	✓	✓	✓	D	✓	✓	10.8	11.5	0.44
SW13	ASW00047ae	J022805.6–051733	0.4	✗	✗	✗	LQ	✗	✗	11.1	11.9	0.46
SW14	ASW0004xjk	J023123.2–082535	–	✗	✗	✗	SQ	✗	✓	–	–	–
SW15	ASW0004nan	J084841.0–045237	0.3	✗	✓	✗	LQ	✓	✓	10.7	11.6	0.59
SW16	ASW0009bp2	J140030.2+574437	0.4	✗	✗	✓	D	✗	✓	11.3	12.1	0.34
SW17	ASW0005rnb	J140622.9+520942	0.7	✓	✗	✗	D	✗	✓	11.1	12.0	0.44
SW18	ASW0007hu2	J143658.1+533807	0.7	✓	✗	✓	D	✗	✗	11.4	12.1	0.31
SW19	ASW0001d7	J020642.0–095157	0.2	✗	✓	✗	IQ	✗	✓	9.6	11.1	0.84
SW20	ASW0002dx7	J021221.1–105251	0.3	✓	✓	✓	IQ	✗	✓	11.2	12.0	0.44
SW21	ASW0004m3x	J022533.3–053204	0.5	✓	✗	✗	D	✗	✓	11.1	11.5	0.24
SW22	ASW0009ab8	J022716.4–105602	0.4	✗	✗	✗	D	✗	✓	11.7	12.1	0.15
SW23	ASW0003r61	J023008.6–054038	0.6	✗	✓	✗	SQ	✗	✓	11.2	12.6	0.71
SW24	ASW00050sk	J023315.2–042243	0.7	✗	✓	✗	LQ	✓	✓	11.4	11.8	0.19
SW25	ASW00007mq	J090308.2–043252	–	✗	✗	✓	D	✗	✓	–	–	–
SW26	ASW0005ma2	J135755.8+571722	0.8	✓	✗	✓	D	✗	✗	11.4	12.3	0.43
SW27	ASW0006jh5	J141432.9+534004	0.7	✗	✗	✗	LQ	✗	✓	10.7	11.7	0.67
SW28	ASW0007xrs	J143055.9+572431	0.7	✗	✓	✗	LQ	✓	✓	11.5	12.1	0.23
SW29	ASW0008qsm	J143838.1+572647	0.8	✗	✓	✓	SQ	✓	✓	11.4	12.1	0.31
SW30	ASW0002p8y	J021057.9–084450	–	✓	✗	✗	IQ	✗	✗	–	–	–
SW31	ASW00021r0	J021514.6–092440	0.7	✗	✓	✗	LQ	✓	✓	11.3	12.7	0.65
SW32	ASW0004iye	J022359.8–083651	–	✗	✓	✗	IQ	✓	✓	–	–	–
SW33	ASW0003s0m	J022745.2–062518	0.6	✓	✓	✓	D	✗	✓	10.9	12.1	0.77
SW34	ASW00051ld	J023453.5–093032	0.5	✗	✗	✓	D	✗	✓	10.9	11.9	0.59
SW35	ASW0004wgd	J084833.2–044051	0.8	✗	✓	✗	LQ	✓	✓	11.4	12.1	0.32
SW36	ASW000096t	J090248.4–010232	0.4	✓	✓	✓	D	✗	✓	11.0	12.0	0.56
SW37	ASW0008xq	J143100.2+564603	–	✗	✗	✓	SQ	✓	✓	–	–	–
SW38	ASW0009cp0	J143353.6+542310	0.8	✗	✓	✓	LQ	✓	✓	11.6	12.6	0.42
SW39	ASW0005qiz	J220215.2+012124	–	–	–	–	–	–	–	–	–	–
SW40	ASW0008wmr	J221306.1+014708	–	✗	✓	✓	SQ	✓	✓	–	–	–
SW41	ASW0008xbu	J221519.7+005758	0.4	✓	✗	✓	IQ	✓	✓	10.5	11.8	0.80
SW42	ASW00096rm	J221716.5+015826	0.1	✓	✓	✓	IQ	✓	✓	8.6	11.0	1.04
SW43	ASW0001c3j	J020810.7–040220	1.0	✗	✗	✗	IQ	✗	✓	11.6	12.4	0.34
SW44	ASW0002k40	J021021.5–093415	0.4	✓	✓	✓	D	✓	✓	11.3	12.8	0.76
SW45	ASW00024id	J021225.2–085211	0.8	✗	✓	✓	CQ	✗	✓	11.7	12.6	0.37
SW46	ASW00024q6	J021317.6–084819	0.5	✓	✓	✓	D	✓	✓	10.9	11.8	0.49
SW47	ASW0003r6c	J022843.0–063316	0.5	✓	✗	✓	D	✗	✓	11.2	12.6	0.71
SW48	ASW0000g95	J090219.0–053923	–	✓	✗	✓	D	✓	✓	–	–	–
SW49	ASW00007ls	J090319.4–040146	–	✗	✓	✓	D	✓	✓	–	–	–
SW50	ASW00008a0	J090333.2–005829	–	✓	✗	✓	LQ	✓	✓	–	–	–
SW51	ASW0006eo0	J135724.8+561614	–	✓	✓	✓	D	✗	✓	–	–	–
SW52	ASW0006a07	J140027.9+541028	–	✓	✗	✓	LQ	✓	✓	–	–	–
SW53	ASW0007v1	J141518.9+513915	0.4	✓	✗	✓	D	✗	✓	11.3	12.5	0.56
SW54	ASW0007sez	J142620.8+561356	0.5	✗	✓	✗	CQ	✓	✓	11.1	12.3	0.68
SW55	ASW0007t5y	J142652.8+560001	–	✗	✓	✓	CQ	✓	✗	–	–	–
SW56	ASW0007pga	J142843.5+543713	0.4	✓	✗	✓	D	✗	✗	10.7	12.0	0.80
SW57	ASW0008pag	J143631.5+571131	0.7	✗	✓	✗	LQ	✗	✗	10.9	12.7	1.08
SW58	ASW0007iwp	J143651.6+530705	0.6	✗	✗	✓	SQ	✓	✓	11.4	12.6	0.58
SW59	ASW00085cp	J143950.6+544606	–	✓	✗	✓	D	✓	✓	–	–	–

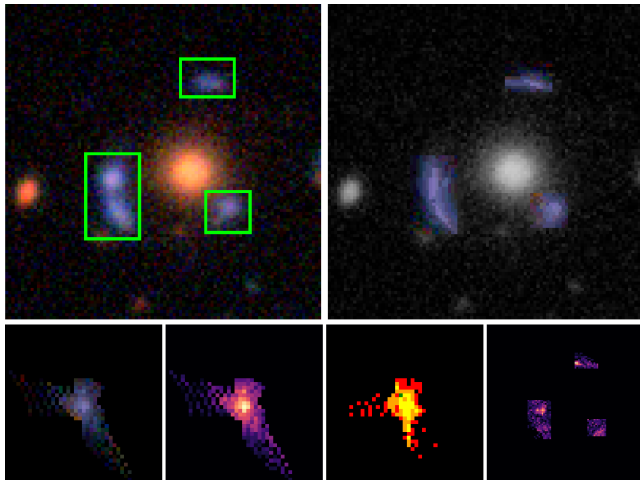


**Figure A1.** Synthetic lensed image with source-profile fitting in SW05 (J143454.4+522850). Top-left: original image, with areas containing lensed images enclosed within green frames. Top-right: synthetic image (coloured arcs) with lensing galaxy and unrelated objects in greyscale. Bottom from left to right: reconstructed source in colour, intensity (greyscale), count of lens plane pixels per source plane pixel, residual of original image to synthetic image.

## APPENDIX A: DEVELOPMENTS IN SPAGHETTILENS

### A1 Improved synthetic images

The mass maps produced by the current implementation of SpaghettiLens are based on images of point-like features. No information about extended images is used, except in so far as they help the user identify images of point-like features. The synthetic images offered to users are rudimentary, corresponding to conical light profiles (*that is, i.e.* circular light profiles with brightness decreasing linearly with radius).

We have now developed a prototype to improve the generation of synthetic images, *as illustrated in Fig. A1*. *Figure A1 illustrates First, areas Areas* containing lensed images are selected (green frames in the figure). The selected areas should be as free as possible from *of light from other sources, including the lensing galaxy or from extraneous objects*. Pixels within the selected areas are mapped to a grid on the source plane, using bending angles given by the mass model. The mapping from lens-plane pixels to source-plane grid cells is many-to-one, because of image multiplicity and magnification. The brightness of each source-plane pixel is set to the mean of all the lens-plane pixels *mapping mapped* to it. Finally, the mapping is run back to the lens plane. The result is a synthetic image. In effect, one is reconstructing a source-plane brightness map by least-squares.

The procedure is not yet implemented in SpaghettiLens but can be applied *in during* post-processing. The new synthetic images could be used to improve the mass reconstruction, by *weighting weighing* the ensemble of maps according to how good the synthetic images are, *but we have not attempted to do so as yet*.

### A2 Sub-sampling of the central region

The models of simulated lenses in Küng et al. (2015) showed a tendency to produce density profiles which were too shallow, resulting typically in overestimates of the Einstein radius. Volunteers could already set the size of the pixels by defining the radius of the lens in pixels, *typical values range with typical values* between 8 and 12. *Additionally allowing 12 pixels. Additionally, it was possible to select* smaller mass tiles in the central region, thus allowing the mass profile to rise more steeply near the centre. *These options were suggested as a possible cure. IF: I don't even know what you mean by the last sentence: we*

**Figure A2** shows an experiment with smaller mass tiles in the inner region. Replacing the very central mass tile with 9 smaller tiles allows for steeper central profiles. Doing the same for the 25 innermost mass tiles allows for *still even* steeper central profiles, eliminating the systematic shallowness. *This is, however, still not shallow profiles. However, it does not provide* a completely satisfactory solution, because (a) it increases the number of mass tiles by 40% and significantly increases the computational time, and (b) the square boundary between *area areas* with different tile sizes is rather undesirable. The main modelling work in this paper was, however, done before the experiments with smaller mass tiles was complete. Some of the models presented in this paper apply the intermediate option (corresponding to the middle panel in **Figure A2**) while others use the old system. *The results in this paper, however, mainly concern* We note this paper mainly concerns the enclosed mass in the outer regions, so shallowness in the central region should be inconsequential not be an issue.

### A3 Parametrization of pixel models

In order to fit the set of pixelated models to a single parametrized model, a *program programme* was written that took a parametrized function and subtracted from it the mean and the principal components (PCs) of the data, *which were calculated using classical Principal Component Analysis*. This created the *residuals residual* function. The number of *components used principal components* in the analysis was varied, to test how this affected the output, *and it*. It was found that *using 5 principal components tended to give PCs gave* a reasonable approximation. A masking function was added *which selected selecting* only the data points that fell inside the image of the lens, and the *principal components PCs* were clipped in order to keep the values inside the region of the ensemble *of models*. Any value higher than the clip was set to be the clip value. This was chosen to *be 2.5* because, assuming that the data follows a Gaussian error distribution, almost all the values for the variance should lie between 2 and 3 standard deviations from the mean. Minimising the residuals function produces the set of parameters that fit the parametrized function to the original pixelated ensemble most closely. A least squares fit was used to perform this minimisation. The parametrized model function was obtained from the gravitational potential of an isothermal ellipsoid mass distribution (Keeton 2001). This model is frequently used to describe gravitational lenses *as it tends to fit well with giving good fits to the* observa-

tions. The isothermal ellipsoid model outputs three useful parameters: the radius of the Einstein ring, the ellipticity of the model and the angle of the ellipticity from the vertical, giving the orientation of the galaxy. By applying this model to simulated lenses for which the values of these parameters were already known, it was possible to gain an estimate of the projected assess the accuracy of the results methodology, before applying the model to the candidate lensing galaxies.

Preliminary results on the recovery of Einstein radii are shown in Figure Fig. A3.

This paper has been typeset from a T<sub>E</sub>X/L<sup>A</sup>T<sub>E</sub>X file prepared by the author.

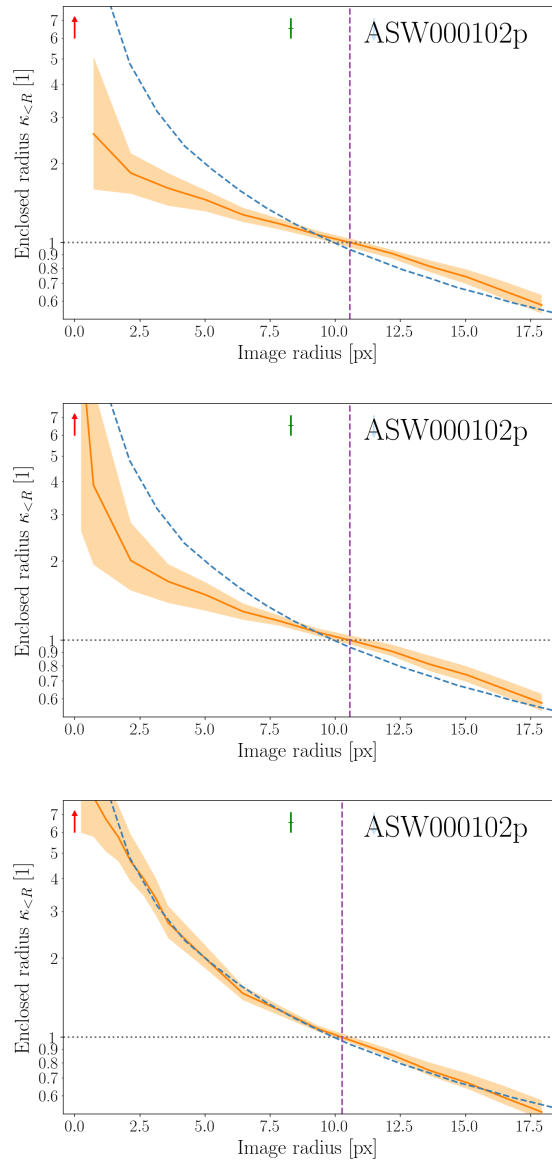


**Figure A2.** Model improvement resulting from using the use of smaller mass tiles in the inner region of the mass model. Shown here are the average enclosed  $\kappa$  within a given projected radius, for three different reconstructions of a simulated lens (sim) from Space Warps. In each panel, the dashed blue curve is the correct answer. The orange band represents the statistical ensemble from SpaghettiLens, the orange line being shows the ensemble mean. Locations of images (maximum, saddle point, minimum) are marked with vertical arrows. Crossing the horizontal The radial value at  $\kappa = 1$  line is the effective Einstein radius,  $r_E$ . The upper panel is taken from Küng et al. (2015), see Figure fig. 3 of that paper. The middle panel is the result when the innermost mass tile is replaced by 9 smaller tiles. The lower panel results from replacing each of the innermost 5 by 5 tiles each with 9 smaller tiles each.

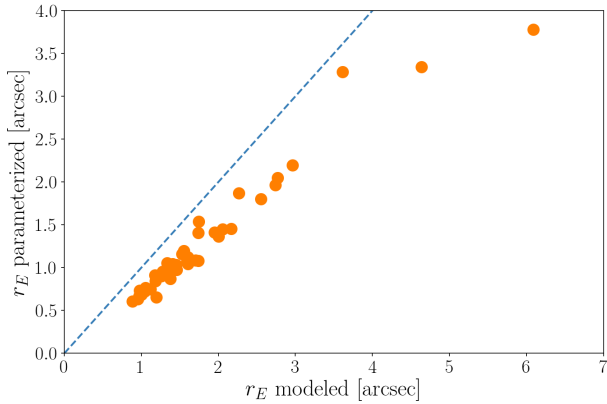


**Figure A3.** Comparison of Einstein radii  $r_E$  obtained from mass tiles directly to those obtained from a parameterized model to test the performance of the parametrization algorithm. The parameterized model was generated using principal component analysis on the ensemble of models. The blue dashed line represents a perfect recovery of  $r_E$ .